

Cover Page



Universiteit Leiden



The handle <http://hdl.handle.net/1887/35116> holds various files of this Leiden University dissertation

**Author:** Punt, Simone

**Title:** The IL-17 and Th17 cell immune response in cervical cancer : angels or demons : it depends on the context

**Issue Date:** 2015-09-08

# VI

## **Whole-transcriptome analysis of flow-sorted cervical cancer samples reveals that B cell expressed TCL1A is correlated with improved survival**

Simone Punt

Willem E. Corver

Sander A.J. van der Zeeuw

Szymon M. Kielbasa

Elisabeth M. Osse

Henk P.J. Buermans

Cornelis D. de Kroon

Ekaterina S. Jordanova

Arko Gorter

*Oncotarget, 2015  
(accepted for publication)*



## Abstract

Cervical cancer is typically well infiltrated by immune cells. Because of the intricate relationship between cancer cells and immune cells, we aimed to identify both cancer cell and immune cell expressed biomarkers for survival. Using a novel approach, we isolated RNA from flow-sorted viable EpCAM<sup>+</sup> tumor epithelial cells and CD45<sup>+</sup> tumor-infiltrating immune cells obtained from squamous cell cervical cancer samples (n=24). Total RNA was sequenced and differential gene expression analysis of the CD45<sup>+</sup> immune cell fractions identified *TCL1A* as a novel marker for predicting improved survival (p=0.007). This finding was validated using qRT-PCR (p=0.005) and partially validated using immunohistochemistry (p=0.083). Importantly, *TCL1A* was found to be expressed in a subpopulation of B cells (CD3<sup>-</sup>/CD19<sup>+</sup>/CD10<sup>+</sup>/CD34<sup>-</sup>). A high *TCL1A/CD20* (B cell) ratio, determined in total tumor samples from a separate patient cohort using qRT-PCR (n=52), was also correlated with improved survival (p=0.027). These results suggest that intratumoral *TCL1A*<sup>+</sup> B cells are important for controlling cervical cancer development.

## Introduction

Cervical cancer is caused by persistent infection with human papillomavirus (HPV) and is currently the second-leading cause of cancer-related death in young women.<sup>1</sup> The prognosis for patients with cervical cancer relapse is poor. Although the host's immune system can usually clear an HPV infection, chronic inflammation can contribute to tumorigenesis.<sup>2</sup> Cervical cancer is characterized by a large number of infiltrating immune cells, and observational and functional studies have revealed that several immune cell types can play a crucial role in the prognosis of patients with cervical cancer. A high number of cytotoxic T cells and T helper type 1 cells is correlated with improved survival in several cancer types,<sup>3,4</sup> including cervical cancer.<sup>5</sup> Cytokines derived from immune cells determine the type of immune response, but they can also directly promote tumor growth.<sup>6</sup> For example, our group and others have shown that a high level of IL-6 expression is an independent predictor of poor survival.<sup>7-9</sup> However, because tumor cells can also produce cytokines and suppress a tumor-targeting immune response,<sup>10</sup> the complex interaction between tumor cells and the local microenvironment makes it challenging to discriminate between effects arising from the tumor cells and effects arising from immune cells.

Because of the intricate relationship between cervical cancer cells and the infiltrating immune cells, the infiltrating immune cells represent an opportunity to identify novel cell-specific biomarkers for improved patient survival. Immunohistochemistry (IHC) is a commonly used method for investigating separate cell types, but is suitable for studying only a select number of strongly expressed antigens. To detect global

differences in gene expression, total RNA is usually studied. However, studying gene expression in tumor samples usually fails to provide information regarding the origin of the cells expressing a particular RNA. Therefore, to distinguish between genes expressed by tumor epithelial cells and genes expressed by tumor-infiltrating immune cells, these two cell subpopulations must first be separated. Although fluorescence-activated cell sorting is a commonly used strategy for selectively identifying cancer stem cells<sup>11-13</sup> and for studying the molecular genetics of tumor cell subpopulations,<sup>14,15</sup> to the best of our knowledge flow cytometry has not been used for transcriptome analysis of matched tumor cell and immune cell subpopulations.

The aim of this study was to discover potential biomarkers for survival expressed by tumor cells or infiltrating immune cells using an unbiased approach. Tumor epithelial cells were separated from immune cells using flow cytometry. Subsequently, we performed total RNA sequencing (RNA-seq) and differential gene expression analysis to examine which genes may play a role in clinical outcome. Our analysis revealed that T-cell leukemia/lymphoma 1A (TCL1A) is a novel immune cell expressed marker for predicting improved survival in patients with cervical cancer. This finding was confirmed using both qRT-PCR and IHC analyses. In addition, we used multicolor immunofluorescence to demonstrate that TCL1A is expressed by a subpopulation of B cells in cervical cancer. This novel approach highlights the potential relevance of tumor infiltrating B cells.

## Materials and Methods

### *Patient material*

Tumor samples were obtained from patients who underwent primary surgical treatment for squamous cell cervical cancer from 1985 through 2005. Samples with sufficient material to dissociate and freeze cells available in the archives of the Department of Pathology (Leiden University Medical Center, Leiden, the Netherlands) were selected for this study (n= 36). None of the patients received preoperative therapy, and clinical and follow-up data were obtained from patient medical records. Samples were handled in accordance with the medical ethical guidelines described in the Code of Conduct for the Proper Secondary Use of Human Tissue established by the Dutch Federation of Biomedical Scientific Societies.

### *Tumor tissue dissociation and sample preparation*

Fresh tumor samples were dissociated as described previously.<sup>16-18</sup> In brief, the tumor tissue was rinsed in RPMI medium (Gibco Life Technologies, Bleiswijk, the Netherlands) and subsequently dissected into 1-2 mm<sup>3</sup> pieces, which were incubated overnight in 10 ml DMEM (Gibco) containing 0.5 mg/ml collagenase type II and

0.002% DNase I type II (both from Sigma-Aldrich, St. Louis, MO). The suspension was then incubated in 0.25% trypsin (Gibco) for up to one hour at 37°C until a single-cell suspension was obtained. The cells were then filtered through a 100-µm pore size nylon sieve (Verseidag-Industrietextilien GmbH, Kempen, Germany), and 10% (v/v) fetal calf serum (FCS) was added. The cells were frozen in 90% FCS/10% DMSO at -180°C until further use.

The protocol for preparing the samples for cell sorting was adapted from Tighe and Matthew.<sup>19</sup> Cell suspensions were thawed rapidly in a 37°C water bath, added to a total volume of 10 ml RPMI medium and centrifuged at 1000xg at 4°C for 3 minutes. The cell pellet was washed in 100 U RNasin Ribonuclease Inhibitor (Promega, Madison, WI) in 1 ml phosphate-buffered saline (PBS), filtered through a 50-µm filter (BD Biosciences, San Jose, CA), stained with haematoxylin and counted. Depending on the total number of cells in each sample, 1-6 million cells were transferred to RNase-free tubes and centrifuged at 800xg at 4°C for 5 minutes. The cell pellets were resuspended in RNasin/PBS, RNasin/PBS containing 1:10 FITC-labelled mouse anti-CD45 antibody (clone T29/33; Dako, Glostrup, Denmark), 1:10 PE-labelled mouse anti-CD326 antibody (i.e., anti-EpCAM; clone EBA-1; BD Biosciences), or RNasin/PBS containing both antibodies. The cells were then incubated in the dark at 4°C for one hour. The samples were washed three times in 1 ml RNasin/PBS by centrifuging at 800xg at 4°C for 5 minutes. The pellets were then resuspended in RNasin/PBS containing 1:4000 TO-PRO-3 (Life Technologies, Carlsbad, CA) and transferred to RNase-free flow cytometry compatible tubes. Identical samples were pooled.

### *Flow cytometry*

A FACSAria IIu (BD Biosciences) was used for cell sorting. Prior to each sorting run, all parts of the sort chamber were cleaned with RNaseZap (Life Technologies), and the inlet tube and flow cell were cleaned with 10% Contrad70 followed by RNasin/PBS. Dead cells were excluded based on TO-PRO-3 staining.<sup>20</sup> Blue and red lasers were used for excitation. A live gate was set using a FSC-A versus TO-PRO-3 fluorescence dot plot. A cut-off of 3% living TO-PRO-3<sup>-</sup> cells was used to exclude samples from further analysis (7 samples exceeded this cut-off and were excluded). Cell doublets were excluded using FSC-H versus FSC-W and SSC-H versus SSC-W pulse-processing. Single-stained samples were used to correct for spectral overlap. EpCAM<sup>+</sup> and CD45<sup>+</sup> single-positive cells in the double-stained samples were sorted using a 16,16 purity mode, a 100-µm nozzle at 20 psi and a drop frequency of 30.8 kHz. A representative example of the restricted gating strategy for sorting pure EpCAM<sup>+</sup> tumor epithelial cells and CD45<sup>+</sup> immune cells is shown in Figure 1. Cells were collected in 2-ml tubes containing 1 ml ice-cold RNeasy Protect Cell Reagent (Qiagen, Hilden, Germany), mixed and kept on ice until RNA isolation.

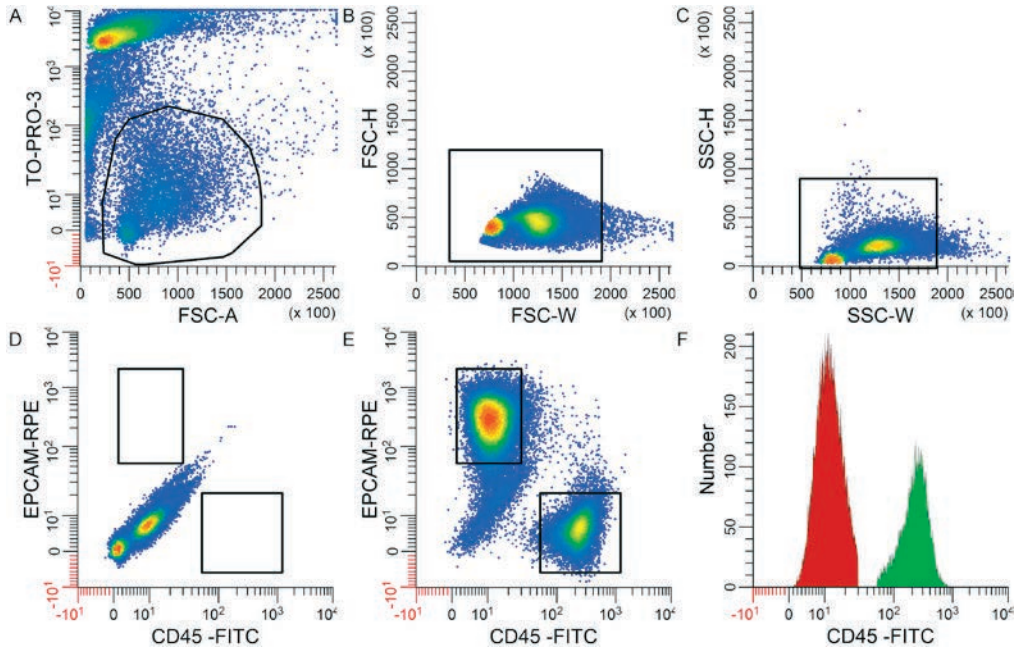


**Figure 1. Example of EpCAM<sup>+</sup> and CD45<sup>+</sup> single-positive cells obtained from a cervical cancer cell suspension using flow cytometry**

The negative control stained for TO-PRO-3 but not for EpCAM or CD45 is shown in A-D. Living cells were selected based on the absence of TO-PRO-3 staining (A), after which cell aggregates were excluded using forward scatter width (B) and side scatter height and width (C). Cell sorting was based on the expression of either EpCAM or CD45 in the double stained samples (E), but not in the unstained control (D). Restricted gates were used as indicated to obtain pure cell populations. Panel (F) shows the distribution of CD45 expression in the CD45<sup>+</sup> immune cells (in green) and the EpCAM<sup>+</sup> tumor cells (in red). Similar results were obtained with respect to EpCAM expression (data not shown).

### Total RNA sequencing

RNA was isolated and DNA was removed using the RNeasy Plus Micro kit (Qiagen). The RNA was eluted from the column using two rounds of 14  $\mu$ l RNase-free water. RNA concentration was measured using a Nanodrop device, and RNA integrity was analyzed using RNA 6000 Pico chips in a model 2100 Bioanalyzer (Agilent Technologies, Santa Clara, CA). A cut-off of 100 ng RNA and an RNA integrity number (RIN) of 8 were used to exclude samples with an insufficient amount of RNA and/or insufficient quality RNA (5 samples were excluded based on these criteria). The mean RIN value of the included samples was 9.2 (range: 8.3-10.0). 20 U RNasin was added to each sample, and the samples were stored at -80°C until use.

External RNA Controls Consortium (ERCC) EXfold spike-in mix (Life Technologies) was added for quality control to 50 ng of total RNA. The RNA was then converted to cDNA and pre-amplified using the SMARTer Ultra Low RNA kit (Clontech Laboratories, Mountain View, CA). A sequencing library was generated from 1 ng

amplified cDNA using the Illumina Nextera XT kit (Illumina, San Diego, CA) as described previously.<sup>21</sup> Paired end 100-base pair sequencing was performed using a HiSeq 2000 v3 (Illumina). FastQ files were generated from each sample using CASAVA version 1.8.2 (Illumina).

### *RNA-seq data analysis*

Sequencing adapters in the FastQ files were detected using FastQC version 0.10.1 and removed using the cutadapt tool (version 1.4.2). Base quality trimming was performed using the sickle tool (version 1.200). RNA was aligned to a custom index based on the hg19 human genome (GSNAP version 2014-05-15; novel splicing flag set to true), supplemented with the ERCC spike-in sequences and replacing the published mitochondrial chromosome with the Revised Cambridge Reference Sequence (GenBank acc. no. NC\_012920\_1). The resulting alignment file was compressed, indexed and name-sorted using the samtools tool (version 0.1.19-44428cd). Reads mapping to ribosomal RNA (obtained from the UCSC rnsk track on the hg19 genome) were removed using a custom-written script. The count table was generated using htseq-count (HTSeq suite version 0.6.1p1; --format flag: BAM; --stranded flag: no; --order flag: name; --mode flag: intersection-nonempty). The UCSC genePredToGtf generated RefSeq annotation (raw database dump of the refGene table) was used as a GTF reference. One of the immune cell fractions was excluded from differential expression analysis because the correlation between the external RNA controls was insufficient ( $r < 0.9$ ).

Differential expression analysis was performed using the R<sup>22</sup> package edgeR.<sup>23</sup> This package uses an overdispersed Poisson model to account for both biological and technical variability. Empirical Bayes methods were used to moderate the degree of overdispersion across transcripts, enhancing the reliability of inference.<sup>23</sup> The values were normalized using the trimmed mean of M (TMM) and the respective library sizes,<sup>24</sup> after which the expression differences between two groups were estimated. Reported p values are false discovery rate–corrected p values calculated using the Benjamini-Hochberg procedure. The Database for Annotation, Visualization, and Integrated Discovery (DAVID; david.abcc.ncifcrf.gov) was used to identify enriched GO terms.<sup>25</sup>

### *qRT-PCR analysis*

RNA was obtained from 52 fresh-frozen squamous cell cervical cancer samples (obtained from 15 patients who were included in the RNA-seq analysis and an additional 37 samples) and is described in chapter 5. cDNA was synthesized as described previously.<sup>26</sup> cDNA was also synthesized from 150 ng of the RNA from the remaining immune cell fractions. The resulting cDNA from the immune cell fractions was purified using the QIAquick PCR Purification Kit (Qiagen). Sybr Green-based

qRT-PCR was performed in duplicate using 1:25 diluted cDNA and 3 pmol RT<sup>2</sup> qPCR Primer Assay for amplifying human *CD19*, *EEF1A1*, *MS4A1* (*CD20*), *RPLP0* and *TCL1A* (Qiagen) on a CFX384 system (Bio-Rad, Hercules, CA). Amplification of *ACTB* was performed using the forward 5'-GCCCTGAGGCACTCTTCCA-3' and reverse 5'-CGGATGTCCACGTCACACTTC-3' primers designed using Primer-BLAST.<sup>27</sup> As a negative control, the cDNA was replaced with milli-Q water. The most stably expressed genes (*EEF1A1* and *RPLP0*) were used for normalization. Expression was scaled by standard deviation. For statistical analysis, gene expression levels were divided into four quartiles, and the lowest quartile (i.e., low expression) was compared with the other three quartiles; in addition, the lower two quartiles were compared with the upper two quartiles.

### *Immunohistochemistry*

Immunostaining was performed as described previously<sup>7</sup> on 4- $\mu$ m thick formalin-fixed, paraffin-embedded (FFPE) sections obtained from the patients included in the RNA-seq analysis. In brief, deparaffinized sections were treated with 0.3% H<sub>2</sub>O<sub>2</sub> in methanol for 20 minutes to block endogenous peroxidase activity. After rehydration, antigen retrieval was performed in 10 mM Tris and 1 mM EDTA (pH 9.0). The samples were incubated in monoclonal rabbit anti-TCL1A (EPR3949, Abcam, Cambridge, UK) diluted in 1% (w/v) bovine serum albumin (BSA) in PBS at room temperature overnight. The samples were then incubated in BrightVision poly-horseradish peroxidase (HRP) anti-mouse/rabbit/rat antibody (Immunologic, Duiven, the Netherlands) at room temperature for 30 minutes. HRP activity was visualized using 3,3'-diamino-benzidine-tetrahydrochloride (DAB+, Dako). The sections were counterstained with haematoxylin and mounted using CV Mount (Leica Biosystems, Newcastle, UK). The number of strong TCL1A<sup>+</sup> cells was counted in two to four hot-spots in the center of the tumor using an Axioskop-20 microscope equipped with a Plan-Neofluar 20x/0.5 objective (Zeiss, Göttingen, Germany), sampling a total tumor area of 1.6-3.1 mm<sup>2</sup> comprising vital tumor epithelium and stroma. For statistical analysis, the number of positive cells was divided into two groups based on the median of 56 cells/mm<sup>2</sup>.

Double- and triple-fluorescent IHC was used to stain TCL1A in combination with mouse IgG1 anti-CD3 (clone F7.2.31, Dako), mouse IgG2b anti-CD8 (clone 4B11, NCL-L-CD8-4B11, Leica Biosystems), mouse IgG1 anti-CD10 (clone 56C6, Dako), mouse IgG1 anti-CD19 (clone 3B10, LifeSpan Biosciences, Seattle, WA), mouse IgG2a anti-CD20 (clone L26, Dako), mouse IgG1 anti-CD34 (clone QBEnd 10, Dako), mouse IgG1 anti-CD79a (clone JCB117, Dako), and/or mouse IgG2a anti-DNTT (clone 41C, Abcam); all incubated at room temperature overnight. The samples were then incubated in a combination of Alexa Fluor-labelled goat anti-rabbit-A488 (A11008), goat anti-mouse IgG1-A647 (A21240), goat anti-mouse IgG2a-A546 (A21133), and/or goat anti-mouse IgG2b-A546 (A21143; all from Life Technologies) at room temperature for one

hour. As negative controls, the primary antibodies were replaced with antibodies of the same isotype with unknown specificity. Images were acquired using an LSM700 confocal laser-scanning microscope equipped with an LCI Plan-Neofluar 25x/0.8 Imm Korr DIC M27 objective (Zeiss). Two to four random images were obtained, sampling a total tumor area of 0.5-1.0 mm<sup>2</sup> comprising vital tumor epithelium and stroma. Double and triple positivity of cells was determined using LSM Image Browser software (version 4.2.0.121, Zeiss). The numbers of TCL1A<sup>+</sup>, CD19<sup>+</sup>, and CD20<sup>+</sup> single-, double-, and triple-positive cells were scored manually in TCL1A<sup>+</sup> cell hot-spots at the center of the tumor using ImageJ version 1.47 (<http://rsb.info.nih.gov/ij>). For statistical analysis, the number of positive cells was divided into two groups based on the median of 43 TCL1A<sup>+</sup> cells/mm<sup>2</sup>, 31 TCL1A<sup>+</sup>CD19<sup>+</sup> cells/mm<sup>2</sup>, 18 TCL1A<sup>+</sup>CD19<sup>+</sup>CD20<sup>+</sup> cells/mm<sup>2</sup> and 5 TCL1A<sup>+</sup>CD19<sup>+</sup>CD20<sup>+</sup> cells/mm<sup>2</sup>.

### *Statistical analysis*

Correlations between qRT-PCR and IHC data and both disease-specific survival and disease-free survival were analyzed using Kaplan-Meier curves in SPSS version 20.0 (IBM, Armonk, NY). Differences in expression between two groups were analyzed using the independent Student's *t*-test. All tests were performed two-sided, and differences with a *p*-value <0.05 were considered statistically significant.

## **Results**

### *Cervical cancer samples*

The patient and tumor characteristics are summarized in Table 1. First, we determined whether our patient cohort (n=24) was representative of the total squamous cervical cancer patient cohort followed from 1985 through 2005 (n=173). The only significant difference identified was increased tumor size in our patient cohort (*p*=0.008), which was due to the requirement for larger tumors to prepare cell suspensions. We found no difference between the study cohort and the other patient samples with respect to survival or postoperative radiotherapy treatment (data not shown).

### *Separation of tumor cell and immune cell fractions*

Following the dissociation of fresh tumor samples, TO-PRO-3<sup>+</sup>EpCAM<sup>+</sup>CD45<sup>-</sup> viable tumor epithelial cells (hereafter referred to as the tumor cell fraction) and TO-PRO-3<sup>-</sup>EpCAM<sup>-</sup>CD45<sup>+</sup> viable immune cells (hereafter referred to as the immune cell fraction) were sorted using flow cytometry (Figure 1). RNA-seq data were obtained from total RNA isolated from both cell fractions. The gene expression pattern in the tumor cell fractions differed considerably from the expression pattern in the immune cell fractions,

**Table 1. Patient and tumor clinico-pathological characteristics**

Clinico-pathological parameter	Category	N = 24 (%)
Age	Median	43
	Range	26-63
FIGO stage <sup>1</sup>	IB	20 (83)
	IIA	4 (17)
TNM stage	IB1	3 (13)
	IB	1 (4)
	IB2	13 (54)
	IIA	5 (21)
	IIB	1 (4)
	IIIA	0 (0)
	IIIB	1 (4)
Lymph nodes	Negative	15 (63)
	Positive	9 (38)
Tumor size (mm) <sup>2</sup>	<40	4 (17)
	≥40	19 (79)
Vaso-invasion	Absent	11 (46)
	Present	13 (54)
Infiltration depth (mm) <sup>2</sup>	<15	8 (33)
	≥15	15 (63)
HPV type	16	13 (54)
	18	5 (21)
	Other	6 (25)

<sup>1</sup>FIGO=Fédération Internationale de Gynécologie et d'Obstétrique

<sup>2</sup>Data were not available for all patients.

as shown by two separate clusters of all tumor cell and immune cell fractions upon performing a principal component analysis of all fractions (Figure 2).

Based on p value ranking, the most upregulated gene in the immune cell fractions was protein tyrosine phosphatase receptor-type C (*PTPRC*,  $p=6.54E-146$ ; Figure 3, Supplementary Table S1), which is also known as *CD45*, the marker used to flow-sort the immune cells. The most significantly enriched biological process Gene Ontology (GO) terms in the immune cell fractions were immune response, leukocyte and lymphocyte terms.

In the tumor cell fractions, the most significantly enriched biological process GO terms were cell cycle, tissue development and cellular process, confirming the identity of this

fraction as well. The most upregulated gene in the tumor cell fractions (i.e., with the lowest p value) was epithelial membrane protein 2 (*EMP2*,  $p=5.49E-36$ ; Figure 3). In addition, another highly significantly upregulated gene was *CDKN2A* (also known as *p16*;  $p=7.08E-25$ ), which is upregulated specifically in cervical cancer cells.

The most strongly differentially expressed genes were upregulated in the immune cell fractions compared with the tumor cell fractions, as shown by the ranking of the 100 most differentially expressed genes (Figure 3).

### Prognostic factors identified in the tumor cell fractions

Within the tumor cell fractions, no genes were significantly differentially expressed based on patient survival status five years after surgery. With respect to lymph node status, membrane metallo-endopeptidase (*MME*; log fold change: 9.1,  $p=0.02$ ) and olfactomedin-like 2A (*OLFML2A*; log fold change: 3.0,  $p=0.02$ ) were expressed at higher levels in patients without lymph node metastases compared with patients with lymph node metastases.

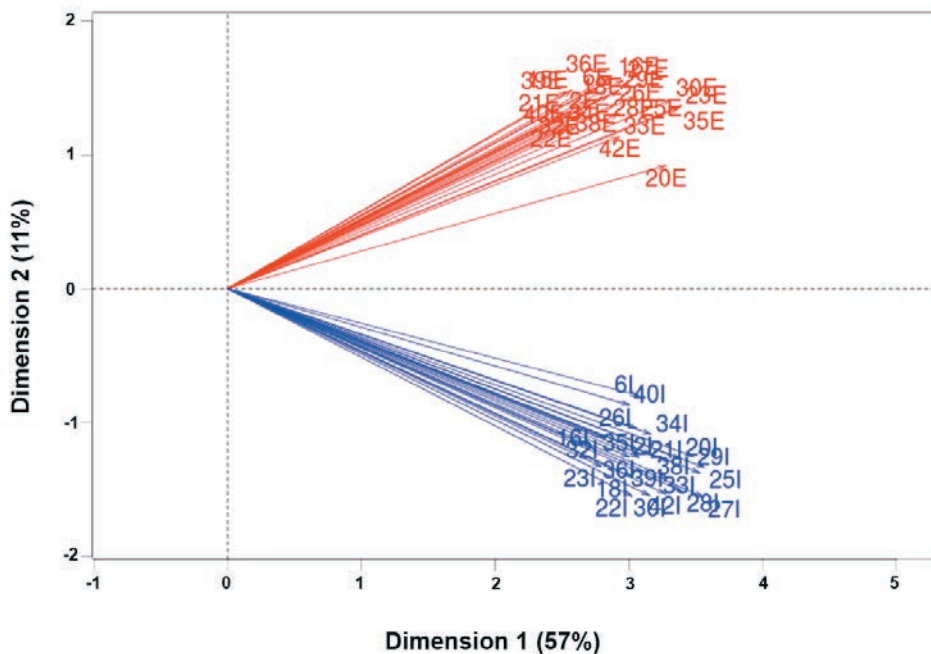


**Figure 2. Principal component analysis of all fractions**

Differential gene expression of the tumor cell fractions and immune cell fractions ( $n=46$ ) obtained from 23 patients (one sample was excluded based on the external RNA controls) was compared using principal component analysis. The numbers indicate the individual patient-matched fractions; “E” indicates a tumor epithelial cell fraction, and “I” indicates an infiltrating immune cell fraction. The percentages in each dimension indicate the amount of variation explained by each dimension. Note that all tumor cell fractions clustered, and all immune cell fractions clustered.

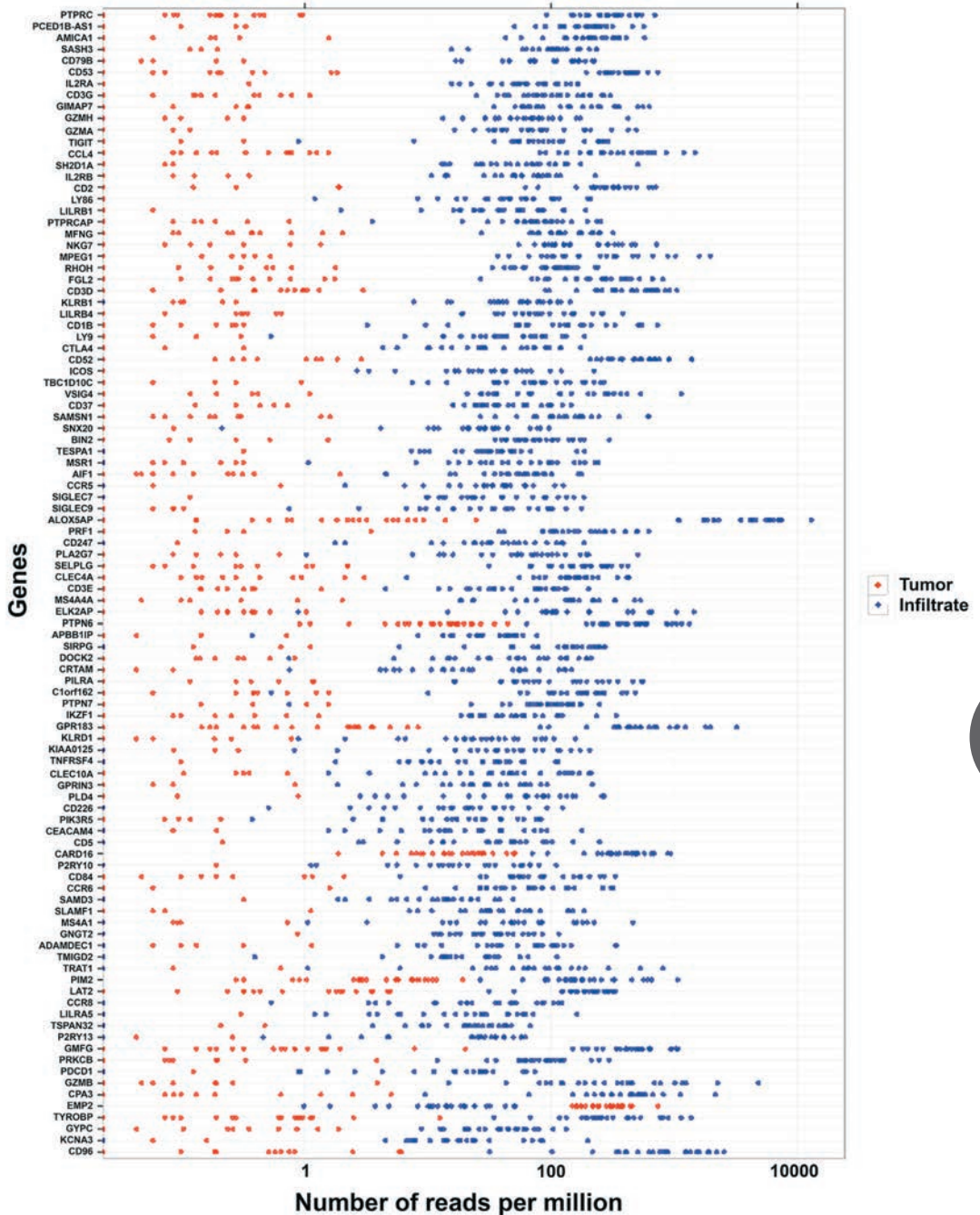


Figure 3. The most differentially expressed genes in the tumor versus the infiltrate fractions

The 100 most significantly differentially expressed genes between the tumor cell (red dots) and infiltrate (blue dots) fractions are shown. The gene with the lowest p value (*PTPRC*) is listed at the top.

## Prognostic factors identified in the immune cell fractions

Among the immune cell fractions, 17 genes were significantly differentially expressed based on patient survival status (Supplementary Table S2 and Supplementary Figure S1). The most prominent gene was *TCL1A*, which encodes a lymphocyte-specific protein. Specifically, *TCL1A* was expressed in the majority of surviving patients, but it was not expressed in any of the patients who died within five years of surgery. Comparing patients with lymph node metastases and patients without lymph node metastases revealed that the expression level of protein phosphatase 3 regulatory subunit 1 (*PPP3R1*) was significantly higher in patients with metastases (log fold change: 5.6,  $p < 0.001$ ), and endothelin 2 (*EDN2*) was expressed only in patients without lymph node metastases (log fold change: 7.0,  $p = 0.03$ ). Because we could best discriminate between patients who survived versus patients who had died based on *TCL1A* expression, we continued to validate the correlation between *TCL1A* expression and patient survival.

## Validation of the correlation between *TCL1A* expression and improved survival

Based on our RNA-seq data, the expression of *TCL1A* was significantly correlated with improved disease-free survival ( $p = 0.047$ ) and disease-specific survival ( $p = 0.007$ ; Figure 4A). To validate the technique used, we performed a qRT-PCR analysis of *TCL1A* expression using the same 24 immune cell fraction RNA samples that were used for generating the RNA-seq data. This analysis confirmed that *TCL1A* was expressed at significantly increased levels in patients who survived compared with patients who died within five years ( $p = 0.0003$ ; Figure 4B). Our qRT-PCR analysis confirmed that *TCL1A* expression was significantly correlated with improved disease-free survival ( $p = 0.033$ ) and improved disease-specific survival ( $p = 0.005$ ), with Kaplan-Meier survival curves that were qualitatively similar to Figure 4A (data not shown).

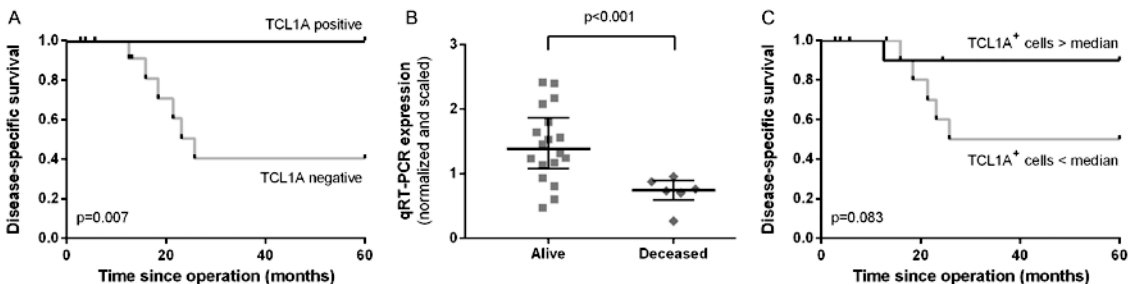


**Figure 4. Correlation between *TCL1A* expression and survival**

A Kaplan-Meier curve and log-rank survival analysis based on the presence or absence of *TCL1A* sequence reads is shown in A. The *TCL1A* qRT-PCR expression values were compared between patients who survived and patients who were deceased five years after surgery in B. The median and interquartile range are depicted. A survival analysis for a high number of *TCL1A*<sup>+</sup> cells versus a low number of *TCL1A*<sup>+</sup> cells based on immunohistochemistry is shown in C.

To validate this correlation at protein expression level, the corresponding FFPE samples were stained for *TCL1A* using IHC. A survival analysis was performed by comparing patients with a high (i.e., above the median of 56 cells/mm<sup>2</sup>) versus a low (i.e., below the median) number of strong *TCL1A*<sup>+</sup> cells (Figure 4C). One patient died despite having a high number of *TCL1A*<sup>+</sup> cells; nevertheless, the data revealed a trend toward improved disease-specific survival (p=0.083).

### *Phenotypic characterization of *TCL1A*<sup>+</sup> cells*

Immunofluorescence staining was used to determine the phenotype of the *TCL1A*<sup>+</sup> cells in FFPE samples from four patients included in the RNA-seq analysis. Strikingly, the *TCL1A*<sup>+</sup> cells did not express CD3 or CD8 (Figure 5A), but the majority of *TCL1A*<sup>+</sup> cells expressed the pan B cell marker CD19 (Figure 5B). Upon further investigation of the B cell phenotype, we found that the majority of *TCL1A*<sup>+</sup> cells also expressed CD10. A smaller population of cells expressed CD20 (Figure 5B,C); relatively few cells expressed CD79a (Figure 5D) or DNA nucleotidylexotransferase (DNTT; Figure 5E), and none of the cells expressed the pro B cell marker CD34 (Figure 5F).

To quantify the relative frequencies of the two predominant *TCL1A*<sup>+</sup> B cell subpopulations (i.e., *TCL1A*<sup>+</sup>CD19<sup>+</sup>CD20<sup>-</sup> and *TCL1A*<sup>+</sup>CD19<sup>+</sup>CD20<sup>+</sup> cells), the numbers of these cell subpopulations were scored in the FFPE samples of all 24 patients who were included in the RNA-seq analysis. On average, 73% of the *TCL1A*<sup>+</sup> cells expressed CD19 (range: 39-95%), and an average of 23% of these *TCL1A*<sup>+</sup>CD19<sup>+</sup> cells also expressed CD20 (range: 0-84%).

Taken together, the majority of *TCL1A*<sup>+</sup> cells expressed CD19 and CD10; in contrast, a minority of cells expressed CD20, and relatively few cells expressed CD79a or DNTT. Most of the DNTT<sup>+</sup> cells did not express CD10. Interestingly, the CD19<sup>+</sup> B cells were distributed throughout the stroma, although some were organized in B cell structures adjacent to tumor epithelial fields.

### *Correlation between B cells, *TCL1A* expression and survival*

We examined the correlations between patient survival and *TCL1A*<sup>+</sup>CD19<sup>+</sup> cells, *TCL1A*<sup>+</sup>CD19<sup>+</sup>CD20<sup>-</sup> cells and *TCL1A*<sup>+</sup>CD19<sup>+</sup>CD20<sup>+</sup> cells on the FFPE samples (n=24). A high (i.e., above the median of 31 cells/mm<sup>2</sup>) number of *TCL1A*<sup>+</sup>CD19<sup>+</sup> cells showed a trend toward improved survival, similar to the correlation for the total number of *TCL1A*<sup>+</sup> cells (see Figure 4C). We found no significant correlation between *TCL1A*<sup>+</sup>CD19<sup>+</sup>CD20<sup>+</sup> cells or *TCL1A*<sup>+</sup>CD19<sup>-</sup>CD20<sup>-</sup> cells and patient survival (data not shown), suggesting that *TCL1A*<sup>+</sup>CD19<sup>+</sup> cells play the most clinically relevant role.

Next, we used qRT-PCR analysis to validate the correlation between *TCL1A* and CD19<sup>+</sup> B cells and improved survival in cervical cancer patients by analyzing the expression levels of *CD19*, *CD20* and *TCL1A* in fresh-frozen cervical cancer samples obtained from 15 patients in the same cohort and an additional 37 samples. We found

no significant correlation between *CD19* expression and disease-specific survival ( $p=0.125$ ; Figure 6A); in contrast, high *CD19* expression was significantly correlated with improved disease-free survival ( $p=0.036$ ; Figure 6B). High expression of *CD3E*, *CD20* or *TCL1A* was not significantly correlated with survival (data not shown), although a high ratio of *TCL1A/CD20* expression showed a trend toward improved disease-specific survival ( $p=0.053$ ).

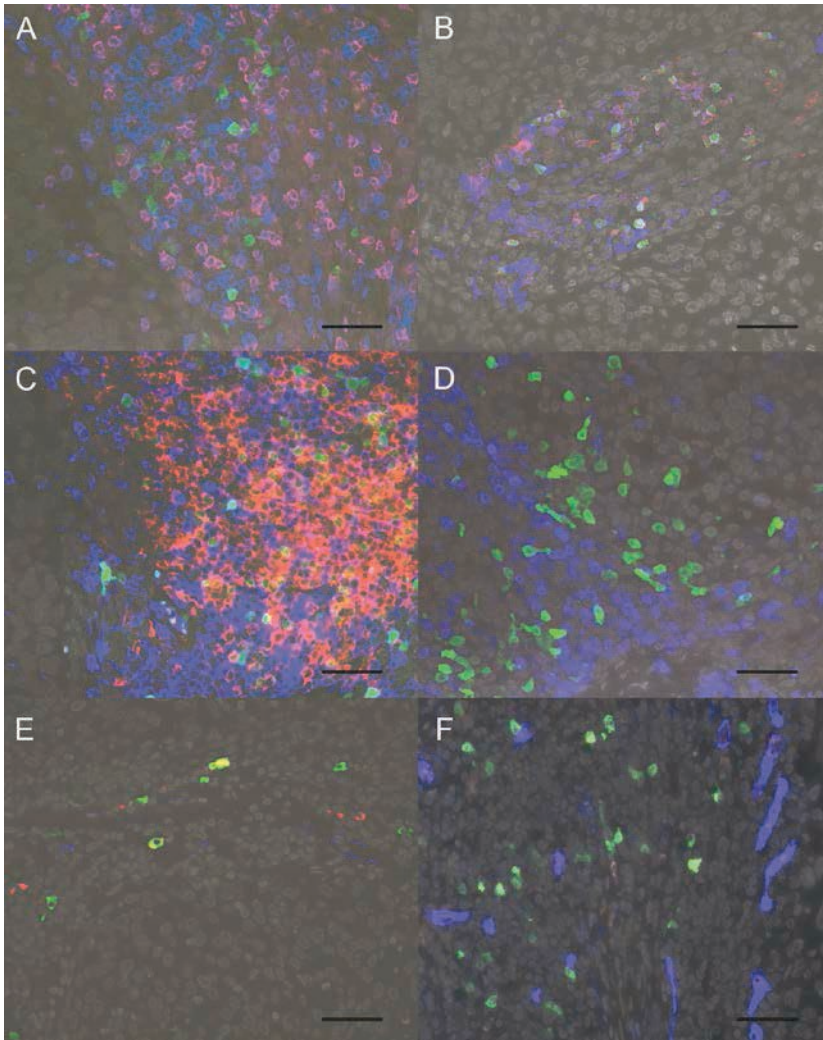


**Figure 5. Phenotype *TCL1A*<sup>+</sup> cells**

A representative image of a squamous cervical cancer FFPE specimen stained for *TCL1A* (green), *CD8* (red) and *CD3* (blue) shows that all *TCL1A*<sup>+</sup> cells were negative for T cell markers (A). A staining for *TCL1A*, *CD20* (red) and *CD19* (blue) indicates that *TCL1A*<sup>+</sup> cells predominantly expressed *CD19*, and part of these cells also expressed *CD20* (purple membrane, B). Similarly, a staining for *TCL1A*, *CD20* and *CD10* (blue) shows that the majority of the *TCL1A*<sup>+</sup> cells expressed *CD10* and part expressed *CD20* (C). Few *TCL1A*<sup>+</sup> cells were found to express *CD79a* (blue, D). An example of infrequent *TCL1A*<sup>+</sup> cells expressing *DNTT* (red) is shown in E (*CD10* is shown in blue). *TCL1A*<sup>+</sup> cells did not express *CD34* (blue, F). In all panels, the nuclei were counterstained with *DAPI* (shown in gray), and the scale bar represents 50  $\mu\text{m}$ .

Based on a quartile division, a low ratio (i.e., the lowest quartile) of *TCL1A/CD20* expression was significantly correlated with poor disease-specific survival ( $p=0.027$ ; Figure 6C) and showed a trend toward poor disease-free survival ( $p=0.051$ ; Figure 6D). Lastly, the ratio of *TCL1A/CD19* expression was not significantly correlated with survival.

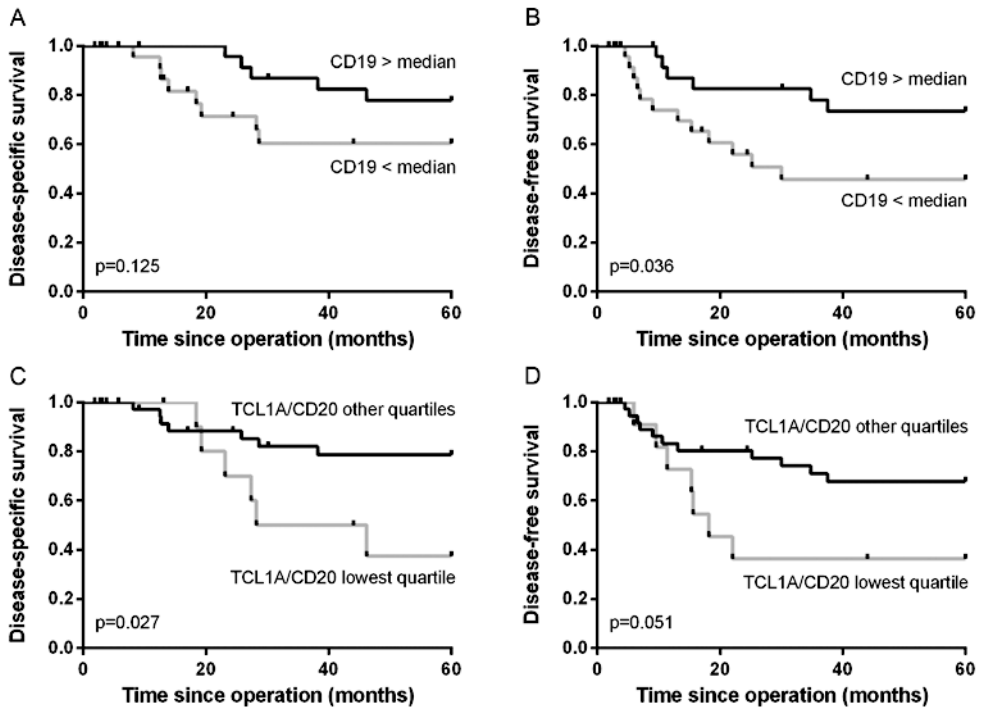


**Figure 6. B cell and *TCL1A* correlations with survival**

Kaplan-Meier analyses are shown based on qRT-PCR analyses of fresh-frozen tumor samples. The correlation between high versus low *CD19* expression and disease-specific (A) and disease-free survival (B) is shown. The ratio of *TCL1A/CD20* expression levels was divided in quartiles. The correlation between the lowest versus the other three quartiles and disease-specific (C) and disease-free (D) survival is shown.

## Discussion

Tumors contain several cell types, including tumor cells, fibroblasts, endothelial cells and infiltrating immune cells. This heterogeneous nature of tumors can complicate the expression analysis of cell subpopulations in the tumor. Here, we report the first study in which RNA was isolated separately from viable tumor epithelial cells and tumor-infiltrating immune cells using flow-sorted fresh-dissociated squamous cell cervical carcinomas. Our aim was to use this novel approach in an attempt to identify factors that are correlated with the clinical outcome of cervical cancer patients.

Differential gene expression analysis of the RNA-seq data revealed that the expression profile in the tumor cell fractions differed from the expression profile in the immune cell fractions. In addition, the most differentially expressed genes matched the epithelial cell and leukocyte origins of the flow-sorted fractions, thus validating the study approach. Interestingly, the most significantly differentially expressed genes were upregulated in the immune cell fractions as compared with the tumor cell fractions. One possible explanation for this finding is that the immune cells in these tumors are a highly heterogeneous population of cells characterized by a higher number of function-specific proteins. The tumor epithelial cells on the other hand might represent a more homogeneous cell population characterized by a more uniform set of proteins.

Our novel approach identified *TCL1A* as a novel putative biomarker for predicting survival in patients with cervical cancer. Specifically, *TCL1A* was not expressed in the immune cell fractions of the deceased patients. We validated the correlation between high *TCL1A* expression and improved survival using both qRT-PCR and IHC analyses. Despite the relatively small number of patients in our study, *TCL1A* expression was robustly correlated with improved survival in the flow-sorted immune cell fractions. A clear trend toward improved prognosis was also found based on the number of *TCL1A*<sup>+</sup> cells in the FFPE samples obtained from the same patients that were included in our RNA-seq analysis. Noh *et al.* reported the presence of *TCL1A* protein in cervical cancer cells,<sup>28</sup> which we did not observe in our patient samples. The reason for this discrepancy might be the use of different antibodies. Since that study did not find a correlation between *TCL1A* expression and survival, strong lymphocyte-specific expression might be specifically correlated with patient survival.

*TCL1A* is expressed in immature CD4<sup>+</sup>CD8<sup>-</sup> T cells and in several stages of developing B cells, including pre-B cells, virgin, mantle and germinal center B cells.<sup>29-31</sup> *TCL1A* is also expressed in activated peripheral lymphocytes, promoting cell proliferation and survival by activating protein kinase B (Akt).<sup>32</sup> In humans and mice, overexpression of *TCL1A* due to chromosomal rearrangement of the *TCL1A* gene to the T cell receptor locus causes mature T cell leukemia and lymphoma.<sup>33,34</sup> Indeed, *TCL1A* overexpression is a common finding in both leukemia and lymphoma,<sup>34</sup> although amplification of this gene was also reported in a pre-malignant cervical lesion.<sup>35</sup> In addition, Hoyer *et al.* showed that *TCL1A* expression induces proliferation by increasing T cell receptor signaling in mature T cells.<sup>36</sup> We found that *TCL1A* was not expressed by T cells in our patient samples. In contrast, *TCL1A* was expressed predominantly in CD19<sup>+</sup> and CD10<sup>+</sup>, CD34<sup>-</sup> B cells. Some of these cells also expressed CD20 and—in rare cases—some cells expressed CD79a or the pro/pre B cell marker DNTT. Based on these markers, we conclude that the *TCL1A*<sup>+</sup> B cells seem to be predominantly germinal center or mature B cells, as well as a subpopulation of pre or immature B cells.

Specifically, the presence of *TCL1A*<sup>+</sup>CD19<sup>+</sup> cells was correlated with a trend toward improved survival. Remarkably, high *CD19* expression was significantly correlated with improved disease-free survival (based on fresh-frozen tumor tissue samples

obtained from an additional cervical cancer patient cohort), whereas *CD3E*, *CD20* and *TCL1A* were not significantly correlated with survival. A low ratio of *TCL1A/CD20* expression was significantly correlated with poor disease-specific survival, indicating that high *TCL1A* expression relative to the expression of the B cell marker *CD20* in total tumor samples is correlated with improved survival. These results suggest that  $CD19^+$  B cells are an important determinant of clinical outcome, and they suggest that the  $TCL1A^+$  and  $CD20^+$  B cell populations play an essential role in this outcome. Further validation on an independent patient cohort is required for *TCL1A* to be used as a prognostic marker.

$TCL1A^+$  B cells were distributed throughout the stroma, although they were also organized in B cell structures located adjacent to tumor epithelial fields. We speculate that  $TCL1A^+$  B cells might indicate lymphoid follicular processes that facilitate B cell maturation, somatic hypermutation and isotype switching. Recently, intratumoral lymphoid structures were reported in several types of cancer,<sup>37,38</sup> and the presence of these structures was correlated with improved survival.<sup>39,40</sup> Compared to T cells, the role of B cells in cancer has been studied less extensively and is controversial. In addition to producing antibodies, tumor-infiltrating B cells can also function as antigen-presenting cells.<sup>41</sup> In melanoma and breast cancer mouse models,  $CD19^+CD20^+CD137L^+$  B cells were reported to activate cytotoxic T cells.<sup>42,43</sup> High numbers of tumor-infiltrating B cells have been correlated with improved patient survival in several cancer types.<sup>44,45</sup> Moreover, antibodies can undergo antigenic selection and affinity maturation in cervical cancer.<sup>46</sup> Our data indicate that intratumoral B cells may play an important role in controlling cervical cancer, and *TCL1A* is a potential marker for a beneficial B cell response.

Based on both positive lymph nodes and death by disease, *PPP3R1* was the most upregulated gene in the immune cell fractions. *PPP3R1* encodes a regulatory subunit of calcineurin, which activates the transcription factor NFAT (nuclear factor of activated T cells).<sup>47</sup> In addition, the vasoconstrictor endothelin 2 was expressed only in the immune cell fractions of patients without lymph node metastases. Because the expression levels of these two genes were inadequate for discriminating between patients and did not differ significantly within the tumor cell fractions, we did not pursue these proteins as potential targets.

With respect to the tumor cell fractions, the only significantly increased expression was observed in the genes *MME* and *OLFML2A* in the patients without lymph node metastases. This low number of differentially expressed genes suggests that the tumor cell fractions were highly homogeneous. We could thus not identify a differential expression pattern based on positive lymph nodes or death by disease. Because of this relative homogeneity, we believe that this technique is a promising tool for identifying pathways that are specific to different cancer types.

In summary, we report that RNA-seq data can be analyzed reliably using tumor cells and immune cells isolated from cancer samples using flow cytometry. The most

distinguishing gene identified by differential expression analysis was *TCLIA*. Specifically, *TCLIA* was not expressed in the immune cells of patients who died from cervical cancer. This correlation between *TCLIA* expression and improved survival was validated using qRT-PCR and IHC analyses. We also found that *TCLIA* was predominantly expressed in B cells, possibly reflecting intratumoral lymphoid follicular processes. Based on these findings, we conclude that *TCLIA* may be a prognostic biomarker for predicting improved survival in patients with cervical cancer. This is the first study demonstrating the prognostic value of separating tumor epithelial cells from tumor-infiltrating immune cells and determining their RNA expression profile for identifying putative cancer biomarkers. Because B cell expressed *TCLIA* was the most prominent marker correlated with patient survival, perhaps we should broaden our T cells biased view to include B cells in cancer immunology. The emerging interest in cancer immunotherapy supports studying the use of B cells in anticancer treatments.

## Acknowledgements

We thank Jaap D.H. van Eendenburg (Department of Pathology, Leiden University Medical Center) for dissociating and freezing the tumor samples, and we thank and Dr. Patty M. Jansen (Department of Pathology, Leiden University Medical Center) for consultation regarding the B cell phenotypes.

## References

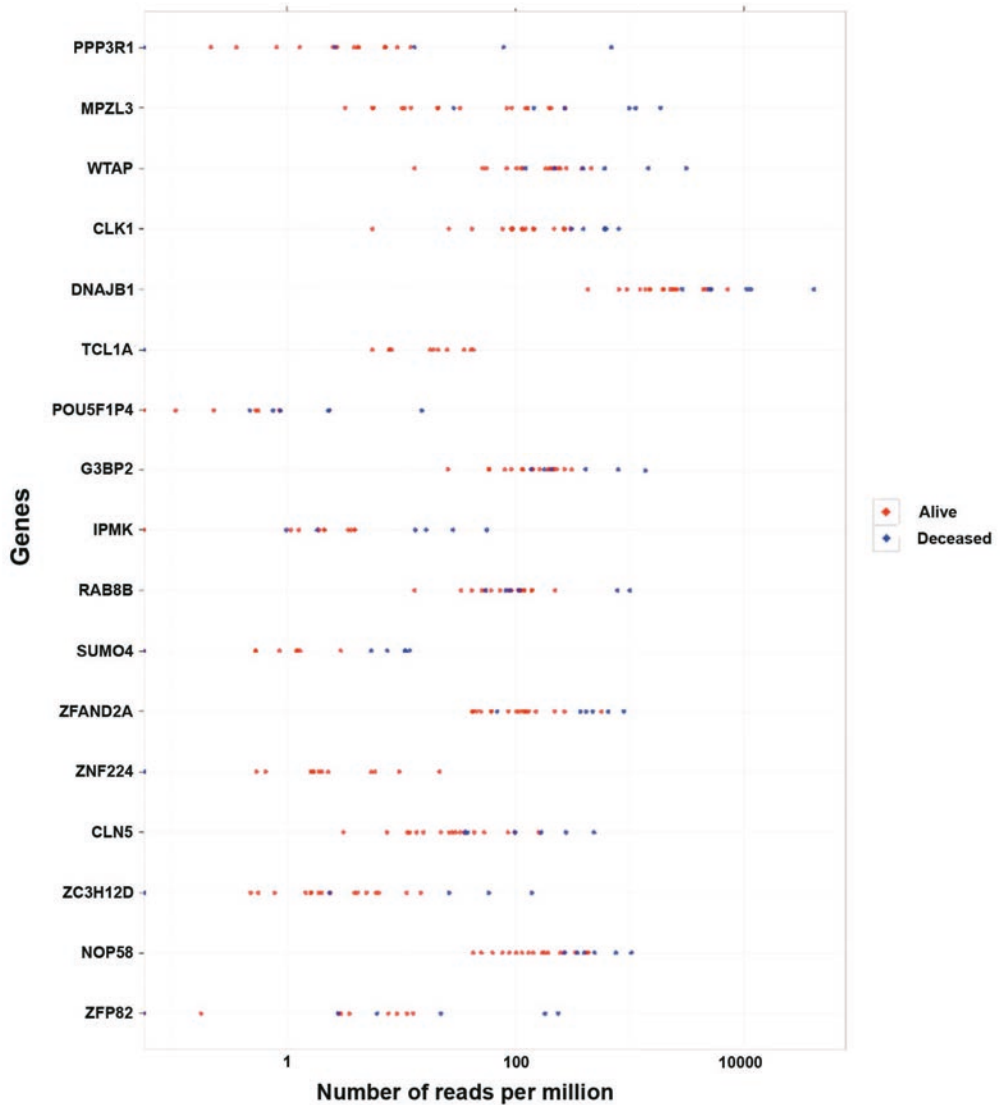
- 1 Siegel R, Ma J, Zou Z, Jemal A. Cancer statistics, 2014. *CA Cancer J. Clin.* 2014; 64: 9-29.
- 2 Balkwill F, Mantovani A. Inflammation and cancer: back to Virchow? *Lancet* 2001; 357: 539-45.
- 3 Ali HR, Provenzano E, Dawson SJ, Blows FM, Liu B, Shah M, Earl HM, Poole CJ, Hiller L, Dunn JA *et al.* Association between CD8+ T-cell infiltration and breast cancer survival in 12,439 patients. *Ann. Oncol.* 2014; 25: 1536-43.
- 4 Fridman WH, Pages F, Sautes-Fridman C, Galon J. The immune contexture in human tumours: impact on clinical outcome. *Nat. Rev. Cancer* 2012; 12: 298-306.
- 5 Jordanova ES, Gorter A, Ayachi O, Prins F, Durrant LG, Kenter GG, van der Burg SH, Fleuren GJ. Human leukocyte antigen class I, MHC class I chain-related molecule A, and CD8+/regulatory T-cell ratio: which variable determines survival of cervical cancer patients? *Clin. Cancer Res.* 2008; 14: 2028-35.
- 6 Mantovani A. Cancer: Inflaming metastasis. *Nature* 2009; 457: 36-7.
- 7 Zijlmans HJ, Punt S, Fleuren GJ, Trimpos JB, Kenter GG, Gorter A. Role of IL-12p40 in cervical carcinoma. *Br. J. Cancer* 2012; 107: 1956-62.
- 8 Duffy SA, Taylor JM, Terrell JE, Islam M, Li Y, Fowler KE, Wolf GT, Teknos TN. Interleukin-6 predicts recurrence and survival among head and neck cancer patients. *Cancer* 2008; 113: 750-7.

- 9 Chen MF, Chen PT, Lu MS, Lin PY, Chen WC, Lee KD. IL-6 expression predicts treatment response and outcome in squamous cell carcinoma of the esophagus. *Mol. Cancer* 2013; 12: 26.
- 10 Stewart TJ, Abrams SI. How tumours escape mass destruction. *Oncogene* 2008; 27: 5894-903.
- 11 Ho DW, Yang ZF, Yi K, Lam CT, Ng MN, Yu WC, Lau J, Wan T, Wang X, Yan Z *et al.* Gene expression profiling of liver cancer stem cells by RNA-sequencing. *PLoS One* 2012; 7: e37159.
- 12 Van den Broeck A, Vankelecom H, Van DW, Gremeaux L, Wouters J, Allemeersch J, Govaere O, Roskams T, Topal B. Human pancreatic cancer contains a side population expressing cancer stem cell-associated and prognostic genes. *PLoS One* 2013; 8: e73968.
- 13 Birnie R, Bryce SD, Roome C, Dussupt V, Droop A, Lang SH, Berry PA, Hyde CF, Lewis JL, Stower MJ *et al.* Gene expression profiling of human prostate cancer stem cells reveals a pro-inflammatory phenotype and the importance of extracellular matrix interactions. *Genome Biol.* 2008; 9: R83.
- 14 Corver WE, Ter Haar NT, Fleuren GJ, Oosting J. Cervical carcinoma-associated fibroblasts are DNA diploid and do not show evidence for somatic genetic alterations. *Cell Oncol. (Dordr. )* 2011; 34: 553-63.
- 15 Corver WE, Ter Haar NT. High-resolution multiparameter DNA flow cytometry for the detection and sorting of tumor and stromal subpopulations from paraffin-embedded tissues. *Curr. Protoc. Cytom.* 2011; Chapter 7: Unit 7.37.
- 16 Hilders CG, Ras L, van Eendenburg JD, Nooyen Y, Fleuren GJ. Isolation and characterization of tumor-infiltrating lymphocytes from cervical carcinoma. *Int. J. Cancer* 1994; 57: 805-13.
- 17 Corver WE, Koopman LA, van der Aa J, Regensburg M, Fleuren GJ, Cornelisse CJ. Four-color multiparameter DNA flow cytometric method to study phenotypic intratumor heterogeneity in cervical cancer. *Cytometry* 2000; 39: 96-107.
- 18 Corver WE, Koopman LA, Mulder A, Cornelisse CJ, Fleuren GJ. Distinction between HLA class I-positive and -negative cervical tumor subpopulations by multiparameter DNA flow cytometry. *Cytometry* 2000; 41: 73-80.
- 19 Tighe S, Held MA. Isolation of total RNA from transgenic mouse melanoma subsets using fluorescence-activated cell sorting. *Methods Mol. Biol.* 2010; 632: 27-44.
- 20 Corver WE, Cornelisse CJ. Flow cytometry of human solid tumours: clinical and research applications. *Current Diagnostic Pathology* 2002; 8: 249-67.
- 21 Picelli S, Faridani OR, Bjorklund AK, Winberg G, Sagasser S, Sandberg R. Full-length RNA-seq from single cells using Smart-seq2. *Nat. Protoc.* 2014; 9: 171-81.
- 22 R Core Team (2014). R: A language and environment for statistical computing. R Foundation for Statistical Computing, Vienna, Austria, 2014.
- 23 Robinson MD, McCarthy DJ, Smyth GK. edgeR: a Bioconductor package for differential expression analysis of digital gene expression data. *Bioinformatics.* 2010; 26: 139-40.
- 24 Robinson MD, Oshlack A. A scaling normalization method for differential expression analysis of RNA-seq data. *Genome Biol.* 2010; 11: R25.
- 25 Dennis G, Jr., Sherman BT, Hosack DA, Yang J, Gao W, Lane HC, Lempicki RA. DAVID: Database for Annotation, Visualization, and Integrated Discovery. *Genome Biol.* 2003; 4: 3.

- 26 de Boer MA, Jordanova ES, Kenter GG, Peters AA, Corver WE, Trimbos JB, Fleuren GJ. High human papillomavirus oncogene mRNA expression and not viral DNA load is associated with poor prognosis in cervical cancer patients. *Clin. Cancer Res.* 2007; 13: 132-8.
- 27 Ye J, Coulouris G, Zaretskaya I, Cutcutache I, Rozen S, Madden TL. Primer-BLAST: a tool to design target-specific primers for polymerase chain reaction. *BMC. Bioinformatics.* 2012; 13: 134.
- 28 Noh KH, Kim BW, Song KH, Cho H, Lee YH, Kim JH, Chung JY, Kim JH, Hewitt SM, Seong SY *et al.* Nanog signaling in cancer promotes stem-like phenotype and immune evasion. *J. Clin. Invest* 2012; 122: 4077-93.
- 29 Takizawa J, Suzuki R, Kuroda H, Utsunomiya A, Kagami Y, Joh T, Aizawa Y, Ueda R, Seto M. Expression of the TCL1 gene at 14q32 in B-cell malignancies but not in adult T-cell leukemia. *Jpn. J. Cancer Res.* 1998; 89: 712-8.
- 30 Narducci MG, Pescarmona E, Lazzeri C, Signoretti S, Lavinia AM, Remotti D, Scala E, Baroni CD, Stoppacciaro A, Croce CM *et al.* Regulation of TCL1 expression in B- and T-cell lymphomas and reactive lymphoid tissues. *Cancer Res.* 2000; 60: 2095-100.
- 31 Virgilio L, Narducci MG, Isobe M, Billips LG, Cooper MD, Croce CM, Russo G. Identification of the TCL1 gene involved in T-cell malignancies. *Proc. Natl. Acad. Sci. U. S. A* 1994; 91: 12530-4.
- 32 Laine J, Kunstle G, Obata T, Sha M, Noguchi M. The protooncogene TCL1 is an Akt kinase coactivator. *Mol. Cell* 2000; 6: 395-407.
- 33 Virgilio L, Lazzeri C, Bichi R, Nibu K, Narducci MG, Russo G, Rothstein JL, Croce CM. Deregulated expression of TCL1 causes T cell leukemia in mice. *Proc. Natl. Acad. Sci. U. S. A* 1998; 95: 3885-9.
- 34 Pekarsky Y, Hallas C, Croce CM. The role of TCL1 in human T-cell leukemia. *Oncogene* 2001; 20: 5638-43.
- 35 Hidalgo A, Baudis M, Petersen I, Arreola H, Pina P, Vazquez-Ortiz G, Hernandez D, Gonzalez J, Lazos M, Lopez R *et al.* Microarray comparative genomic hybridization detection of chromosomal imbalances in uterine cervix carcinoma. *BMC Cancer* 2005; 5: 77.
- 36 Hoyer KK, Herling M, Bagrintseva K, Dawson DW, French SW, Renard M, Weinger JG, Jones D, Teitell MA. T cell leukemia-1 modulates TCR signal strength and IFN-gamma levels through phosphatidylinositol 3-kinase and protein kinase C pathway activation. *J. Immunol.* 2005; 175: 864-73.
- 37 Bergomas F, Grizzi F, Doni A, Pesce S, Laghi L, Allavena P, Mantovani A, Marchesi F. Tertiary intratumor lymphoid tissue in colo-rectal cancer. *Cancers. (Basel)* 2011; 4: 1-10.
- 38 Coronella JA, Spier C, Welch M, Trevor KT, Stopeck AT, Villar H, Hersh EM. Antigen-driven oligoclonal expansion of tumor-infiltrating B cells in infiltrating ductal carcinoma of the breast. *J. Immunol.* 2002; 169: 1829-36.
- 39 Dieu-Nosjean MC, Antoine M, Danel C, Heudes D, Wislez M, Poulot V, Rabbe N, Laurans L, Tartour E, de CL *et al.* Long-term survival for patients with non-small-cell lung cancer with intratumoral lymphoid structures. *J. Clin. Oncol.* 2008; 26: 4410-7.
- 40 Dieu-Nosjean MC, Goc J, Giraldo NA, Sautes-Fridman C, Fridman WH. Tertiary lymphoid structures in cancer and beyond. *Trends Immunol.* 2014; 35: 571-80.

- 41 Namm JP, Li Q, Lao X, Lubman DM, He J, Liu Y, Zhu J, Wei S, Chang AE. B lymphocytes as effector cells in the immunotherapy of cancer. *J. Surg. Oncol.* 2012; 105: 431-5.
- 42 Bodogai M, Lee CC, Wejksza K, Lai J, Merino M, Wersto RP, Gress RE, Chan AC, Hesdorffer C, Biragyn A. Anti-CD20 antibody promotes cancer escape via enrichment of tumor-evoked regulatory B cells expressing low levels of CD20 and CD137L. *Cancer Res.* 2013; 73: 2127-38.
- 43 Lee-Chang C, Bodogai M, Moritoh K, Olkhanud PB, Chan AC, Croft M, Mattison JA, Holst PJ, Gress RE, Ferrucci L *et al.* Accumulation of 4-1BBL+ B cells in the elderly induces the generation of granzyme-B+ CD8+ T cells with potential antitumor activity. *Blood* 2014; 124: 1450-9.
- 44 Meshcheryakova A, Tamandl D, Bajna E, Stift J, Mittlboeck M, Svoboda M, Heiden D, Stremitzer S, Jensen-Jarolim E, Grunberger T *et al.* B cells and ectopic follicular structures: novel players in anti-tumor programming with prognostic power for patients with metastatic colorectal cancer. *PLoS One* 2014; 9: e99008.
- 45 Pelletier MP, Edwardes MD, Michel RP, Halwani F, Morin JE. Prognostic markers in resectable non-small cell lung cancer: a multivariate analysis. *Can. J. Surg.* 2001; 44: 180-8.
- 46 O'Brien PM, Tsirimonaki E, Coomber DW, Millan DW, Davis JA, Campo MS. Immunoglobulin genes expressed by B-lymphocytes infiltrating cervical carcinomas show evidence of antigen-driven selection. *Cancer Immunol. Immunother.* 2001; 50: 523-32.
- 47 McCaffrey PG, Perrino BA, Soderling TR, Rao A. NF-ATp, a T lymphocyte DNA-binding protein that is a target for calcineurin and immunosuppressive drugs. *J. Biol. Chem.* 1993; 268: 3747-52.

Supplementary Figure S1. Differentially expressed genes in infiltrating immune cell fractions based on patient survival status



The significantly differentially expressed genes in the tumor-infiltrating immune cell fractions between patients who were alive (red dots) and patients who were deceased (blue dots) is shown. The gene with the lowest p value (*PPP3R1*) is shown at the top.

Supplementary Tables S1 and S2 were too extended to include in this thesis, and can be obtained from the author.

